

**CORE SOLIDIFICATION AND CONTRACTION ON 16 PSYCHE.** Fiona Nichols-Fleming<sup>1\*</sup>, Alexander J. Evans<sup>1</sup>, and Brandon C. Johnson<sup>2,3</sup>, <sup>1</sup>Department of Earth, Environmental, and Planetary Sciences, Brown University, Providence, RI, USA (\*[fiona\\_nichols-fleming@brown.edu](mailto:fiona_nichols-fleming@brown.edu)), <sup>2</sup>Department of Earth, Atmospheric, and Planetary Sciences, Purdue University, West Lafayette, IN, USA, <sup>3</sup>Department of Physics and Astronomy, Purdue University, West Lafayette, IN, USA.

**Introduction:** Radial contraction has historically been used as a way to infer a planetary body's thermal history based on surface observations of pervasive thrust faulting [e.g., 1–3]. As we look forward to the Psyche mission's arrival at asteroid 16 Psyche in 2029, we can inform our understanding of the relationship between Psyche's thermal history and radial contraction.

M-type asteroids, of which 16 Psyche is the largest [4], are generally hypothesized to have metal-rich surfaces. However, Psyche's inferred density is  $4,000 \pm 200 \text{ kg/m}^3$  [5], which is lower than the uncompressed densities of Mercury, Venus, and Earth. Using the composition of meteoritic metal, this current density estimate would require an iron-nickel Psyche to have a bulk porosity of  $\sim 52 \text{ vol}\%$  [6]. Recent thermal models indicate that a pure iron body must have previously cooled to  $\lesssim 800 \text{ K}$  to retain a  $52 \text{ vol}\%$  porosity [7]. It is currently unclear if a porosity-adding event could occur sufficiently late to allow for these cool temperatures. Alternatively, if a high porosity is not possible, Psyche's metal must be accompanied by a significantly lower density component, such as rock.

For a Psyche-sized body ( $D_{\text{eff}} = 111 \text{ km}$ ) composed of rock and iron, differentiation is likely due to efficient heating by accretion and radioactive decay [e.g., 8,9]. Due to the relatively low pressures within Psyche (a central pressure  $\sim 100 \text{ MPa}$ ), the process of solidification within Psyche's core will differ from that of larger planetary bodies. Rather than at the center of the core, solid core nucleation will occur at the core-mantle boundary [10]. Additionally, analysis of the cooling rates of iron meteorites with varying nickel content indicate that both inward and outward solidification scenarios are possible [11,12], where in this case outward solidification is defined as the growth of a solid inner core due to accumulated iron snow. The intricacies associated with the cooling of small differentiated bodies will ultimately influence the thermal evolution of these bodies and thus the contractional history as well.

Here we investigate the influence of mantle thickness and direction of core solidification on the thermal and contraction history of a Psyche-size body. We find that the direction of solidification influences the early stages of radial contraction within the bodies and thus observed contraction could be used to distinguish between the two scenarios in cases where the first  $\sim 5 \text{ Myr}$  of Psyche's contractional history are preserved. Beyond

this the contraction history can be used to constrain Psyche's mantle thickness and longer timescale cooling.

**Methodology:** To model the thermal evolution of differentiated bodies we use a 1-D forward time, central space finite difference model of thermal conduction coupled with solidification of an isothermal fluid core. An isothermal core is an appropriate simplification as the temperature difference for the appropriate pressure range for the core ( $\lesssim 100 \text{ MPa}$ ) is only  $\sim 2 \text{ K}$ . For simplicity, we assume the initial temperature structure of all models to be an isothermal mantle at  $1300 \text{ K}$  and an isothermal fluid core at  $1820 \text{ K}$ . Additionally, each model has a constant surface temperature of  $137 \text{ K}$ , the average surface temperature of Psyche [13].

The rate of solidification in our models is limited by the rate of core conductive heat transport to the layer immediately above the fluid portion of the core, following [14]. Once the liquid core cools to its melting temperature, for each timestep, the temperature of the fluid core remains constant and the volume of iron solidified is determined by the latent heat equivalent to the core heat loss. After solidification, the iron layer in each model cools conductively.

To determine the radial contraction history appropriate for our models, we include both radial changes due to thermal contraction of the entire body in addition to the volume change due to the phase change from liquid to solid iron within the core. These calculations are described in detail in [1].

**Results & Discussion:** We model the thermal evolution of bodies  $110 \text{ km}$  in radius with mantle thicknesses of  $1, 10, 20,$  and  $50 \text{ km}$  and inward and outward core solidification directions. The full contraction of these models in addition to a conductively cooling porous iron model are shown in Figure 1 where associated mantle thicknesses indicated by line color and core solidification direction is indicated by line style (dashed and solid lines for inward and outward solidification, respectively). The porous iron body is a Psyche-mass body with  $52 \text{ vol}\%$  porosity and an initially uniform temperature of  $600 \text{ K}$ . The total amount of contraction experienced by the bodies is independent of solidification direction and the cool, porous model has the least radial contraction, as expected. The magnitude of total contraction, however, is controlled by the thickness of the mantle, with thicker mantles resulting in lower amounts of total contraction. This relationship is due to

the larger expansion coefficient of iron as well as the larger volume of iron undergoing a phase change in cases with thinner mantles. Thus, observations of the magnitude of radial contraction may help constrain Psyche's mantle thickness.

Additionally, the timing of the onset of core solidification is dependent on the mantle thickness via two factors and ranges from  $\sim 0.10$  to  $\sim 0.27$  Myrs. A thicker mantle is able to insulate the core more effectively and therefore delay the onset of solidification. However, as the total radius of the body remains constant throughout our models, a thicker mantle results in a smaller core volume and therefore a smaller total energy that must be removed from the core to reduce the core temperature to the melting temperature. Due to these factors, we find that the time to the onset of solidification for the 10 km mantle case ( $\sim 0.27$  Myr) is the largest of the four mantle thickness scenarios considered.

The differences in early contraction history for inward and outward solidification in the models with a 10 km mantle are shown in Figure 2. The two models begin solidification at the same time, but outward solidification is completed much earlier than inward solidification (0.28 vs 2.9 Myrs, respectively). This is because, in the case of outward solidification, the conductive lid is only the rocky mantle rather than the mantle and the increasingly thick solid core for the inward solidification case. This difference in solidification timescale broadly agrees with the models of [14]. Due to the rapid solidification of the core in the outward case, the early stage of contraction in these models is dominated by the phase change of iron. In the inward case however, the solidification occurs over a longer timescale and the effects of both phase change and cooling are observed. This leads to differences in the magnitude of contraction for the two solidification directions within the first few million years of our models. As the modeled bodies continue cooling, the two core solidification scenarios approach the same final magnitude of contraction. The inclusion of sulfur within a planetesimal core will prolong solidification timescales for both inward and outward solidification and will be considered in ongoing work.

For bodies that experience large amounts of radial contraction, widespread thrust faulting is expected and analysis of the thrust faults can determine the extent of radial contraction experienced by the body. If the Psyche spacecraft observations find thrust faults and are able to distinguish the early stages of Psyche's contraction, the direction of core solidification could be inferred. Furthermore, the complete record of contraction observed by the Psyche spacecraft can be used to place constraints on 16 Psyche's mantle thickness and cooling history. Alternatively, a lack of thrust faulting on Psyche could suggest a thick mantle, a cool re-accretion

with high porosity, or a surface younger than the predicted ancient thrust faulting.

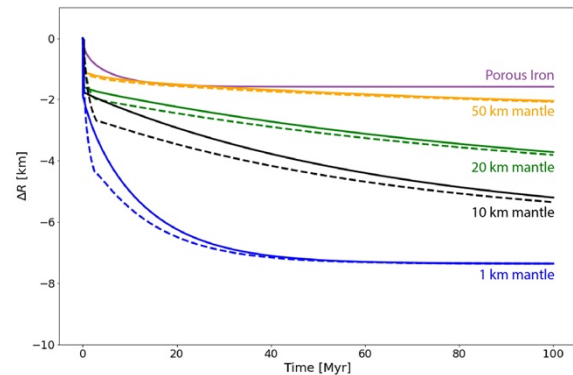


**Figure 1.** Cumulative radial contraction as a function of time for Psyche-sized bodies with mantle thicknesses of 1, 10, 20, and 50 km and a Psyche-mass porous iron body. The colors indicate the mantle thickness of the model and the line style indicates the differences in contraction history for models with inward vs. outward core solidification processes, dashed and solid lines, respectively.

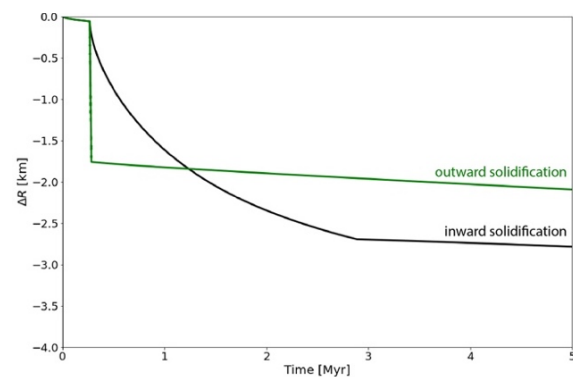


**Figure 2.** Cumulative radial contraction as a function of time within the first 5 Myrs of the model for Psyche-sized bodies with a 10 km thick mantle. Inward and outward solidification directions are shown in black and green, respectively.

**References:** [1] Solomon, S. C. (1977) *Physics of the Earth and Planetary Interiors*, 15, 135–145. [2] Byrne, P. K. et al. (2014) *Nature Geosci*, 7, 301–307. [3] Watters, T. R. (2021) *Commun Earth Environ*, 2, 1–9. [4] Shepard, M. K. et al. (2017) *Icarus*, 281, 388–403. [5] Shepard, M. K. et al. (2021) *PSJ*, 2, 125. [6] Elkins-Tanton, L. T. et al. (2020) *JGR: Planets*, 125, e06296. [7] Nichols-Fleming, F. et al. (2022) *JGR: Planets*, 127, e2021JE007063. [8] Šrámek, O. et al. (2012) *Icarus*, 217, 339–354. [9] Neumann, W. et al. (2012) *A&A*, 543, A141. [10] Williams, Q. (2009) *EPSL*, 284, 564–569. [11] Yang, J. et al. (2008) *Geochimica et Cosmochimica Acta*, 72, 3043–3061. [12] Yang, J. et al. (2010) *Geochimica et Cosmochimica Acta*, 74, 4493–4506. [13] Sori, M. M. et al. (2017) *LPSC 48*, 2550. [14] Scheinberg, A. et al. (2016) *JGR: Planets*, 121, 2–20.